Velocity Profiles in Slowly Sheared Bubble Rafts

John Lauridsen,* Gregory Chanan,† and Michael Dennin
Department of Physics and Astronomy, University of California at Irvine, Irvine, California 92697-4575, USA
(Received 5 December 2003; published 2 July 2004)

Measurements of average velocity profiles in a bubble raft subjected to slow, steady shear demonstrate the coexistence between a flowing state and a jammed state similar to that observed for three-dimensional foams and emulsions [P. Coussot *et al.*, Phys. Rev. Lett. **88**, 218301 (2002)]. For sufficiently slow shear, the flow is generated by nonlinear topological rearrangements. We report on the connection between this short-time motion of the bubbles and the long-time averages. We find that velocity profiles for individual rearrangement events fluctuate, but a smooth, average velocity is reached after averaging over only a relatively few events.

DOI: 10.1103/PhysRevLett.93.018303 PACS numbers: 83.80.Iz, 64.70.Dv, 83.60.La

Many common complex fluids, such as pastes, emulsions, foams, granular materials, and colloidal systems, flow only when the applied stress exceeds a critical value, known as the yield stress. It is common to model the response of such materials to external stress using *continuous* functions of shear rate, such as appear in Bingham and Herschel-Bulkley models [1]. A striking feature of these models is that, as the shear stress or shear rate is reduced, the apparent viscosity (the ratio of shear stress to shear rate) diverges. At the yield stress, there is a transition from a flowing state to a solid, or "jammed," state. Similar diverging viscosities are observed in glasses, where the system "jams" as a function of temperature or density. Both the detailed flow behavior and underlying mechanisms for jamming in yield stress fluids and glasses are the subject of intense research [2]. A recent proposal suggests that a generalized jamming phase diagram can provide a unifying description of the mechanical behavior of this wide class of materials [3]. Experiments have confirmed the applicability of the jamming phase diagram in colloidal systems [4]. Recent reports of a *discontinuous* jamming transition [5–7] raise important issues for our understanding of yield stress materials and the jamming phase diagram concept, both of which have focused on continuous functions of stress and shear rate. More generally, similar discontinuities have been observed for other shear-induced transitions, such as reported in Ref. [8] for the transition between disordered and aligned wormlike micelles, raising the general question of the nature of inhomogeneous flows during shear-induced transitions of complex fluids.

As these materials are typically opaque, quantitative measurements of a velocity distribution require either two-dimensional systems or recently developed techniques, such as magnetic-resonance imaging [6]. Therefore, only recently have quantitative experimental studies of velocity profiles in jammed systems been carried out. These studies have focused on flow in a Couette geometry, i.e., the flow generated between concentric cylinders with either the inner or outer cylinder rotating [6,8–13]. In this geometry, there is often a transition, at a particular radial position, from flowing to jammed behavior. This coexistence of nonzero and zero shear-rate regions is referred to as shear localization. Such inhomogeneous flows are expected for yield stress materials in a Couette geometry [1]. Initial observation of such flows were qualitative [14,15]. Most quantitative measurements reveal an exponential velocity profile [9–12] and a corresponding continuous shear rate. In contrast, the discontinuous jamming transition is characterized by a discontinuity in the shear rate at the transition between the flowing state and the jammed state [6,8,13]. This behavior cannot be understood in the context of standard, continuous models of yield stress materials [1,5].

For slow shear rates, yield stress materials exhibit flow behavior in which the stress fluctuates in an irregular fashion [2,16–18]. Individual particles in the fluid undergo periods of elastic deformation followed by periods of nonlinear rearrangements that release stress (stress drops). Reference [6] focused on the high shear rate, or continuum limit. In this Letter, we report on experimental measurements of a discontinuous jamming transition for slow shear rates using a model two-dimensional system: a bubble raft. The connection between the long-time average of the velocity profiles and the flow during individual nonlinear rearrangements is discussed. We also consider the connection between applied stress and the radial position of the jamming transition.

A bubble raft consists of a single layer of bubbles floating on a fluid surface [19]. In our system, the bubbles were formed by flowing nitrogen through a solution of (by weight) 44% glycerine, 28% Miracle Bubbles (Imperial Toy Corporation), and 28% water. The fluid subphase consisted of the same solution. A random distribution of bubble sizes was used, with an average radius of 1 mm and a maximum radius of 2.5 mm. The gas area fraction was 0.9. Our Couette viscometer is described in detail in Ref. [20]. Shear flow is generated by rotating the outer cylinder at a constant angular velocity Ω. The shear rate is given in terms of the azimuthal velocity $v_\theta(r)$ by

$\dot{\gamma}(r) = r(d/dr)[v_\theta(r)/r]$ [1]. We report on the normalized angular velocity $v(r) = v_\theta(r)/(\Omega r)$. The jammed state is $v(r) = 1$, or $\dot{\gamma}(r) = 0$. The critical radius at which the transition from flow to the jammed state occurs is denoted by r_c. The stress $\sigma(r_i)$ on the inner cylinder of radius r_i was determined from the torque T on the inner cylinder: $\sigma(r_i) = T/(2\pi r_i^2)$. The inner cylinder was supported by a torsion wire (torsion constant $\kappa = 5.7 \times 10^{-7}$ N m), and T was determined from the angular position of the inner cylinder. The inner cylinder had an instantaneous angular speed, but its average angular speed was zero. At *both* boundaries, the first layer of bubbles was never observed to slip relative to the boundary, setting the effective inner ($r_i \approx 4.3$ cm) and outer ($R = 7.2$ cm) radii. We report results for two rotation rates of the outer cylinder, $\Omega = 8 \times 10^{-4}$ rad/s [$\dot{\gamma}(r_i) = 4 \times 10^{-3}$ s^{-1}] and $\Omega = 5 \times 10^{-3}$ rad/s [$\dot{\gamma}(r_i) = 3 \times 10^{-2}$ s^{-1}].

The time-averaged stress $\langle\sigma(r_i)\rangle$ versus $\dot{\gamma}(r_i)$ is reported elsewhere [16]. It is consistent with a Herschel-Bulkley model of viscosity: $\langle\sigma(r_i)\rangle = \mu_o \dot{\gamma}^n(r_i) + \tau_o$, with $n = 1/3$, and $\tau_o = 0.8 \pm 0.1$ mN/m and $\mu_o = 1.8 \pm 0.2$ mNs$^{1/3}$/m. In this model, τ_o is the yield stress. For $\dot{\gamma}(r_i) < 0.1$ s^{-1}, $\langle\sigma(r_i)\rangle$ was essentially constant [16]. Both shear rates reported on here are within this quasistatic limit.

The fluid substrate (subphase) is driven at the same time as the bubbles [20]. With no bubbles in contact with the outer cylinder, rotation of the outer cylinder generates no motion of the bubble raft. This eliminates driving of the bubbles by the subphase as a potential complication. The effective internal viscosity of the bubble raft (30 to 250 kg/m s for the range of $\dot{\gamma}$ studied here) is a factor of 10^4 to 10^5 greater than the viscosity of the subphase. This ensures that dissipation between bubbles dominates subphase-bubble dissipation.

Bubble velocities were measured from digitized, taped video images. For $\Omega = 8 \times 10^{-4}$ rad/s, the time between digitized images was 3.2 s/image and for $\Omega = 5 \times 10^{-3}$ rad/s, it was 2.0 s/image. An image processing routine based on standard National Instruments Labwindows^{TM}/CVI functions detected and tracked individual bubbles. The velocity at each time was calculated using 10 consecutive images. This placed lower limits on the speed measurements of 6×10^{-4} cm/s for $\Omega = 8 \times 10^{-4}$ rad/s and 9×10^{-4} cm/s for $\Omega = 5 \times 10^{-3}$ rad/s. The velocities of bubbles within each of 24 equally spaced radial bands in the range $4.3 \leq r \leq 7.2$ cm were averaged over an angular range of -1 to 1 rad (roughly 1/3 of the system) to compute $v(r)$.

Figure 1 is a plot of $\sigma(r_i)$ versus time for the velocity data reported on here, including the initial linear increase of $\sigma(r_i)$ with time (elastic response). The subsequent "flowing" regime is dominated by irregular variations in the stress characteristic of the slow shear-rate "flow" of many jammed systems [2,16–18]. The various horizontal and vertical lines will be discussed in the context of the measured flow behavior.

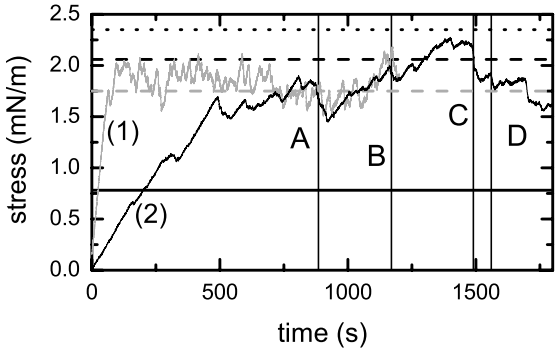

FIG. 1. Stress versus time for $\Omega = 5 \times 10^{-3}$ rad/s [gray line labeled (1)] and $\Omega = 8 \times 10^{-4}$ rad/s [black line labeled (2)]. The solid horizontal line is τ_o determined from a fit using data from Ref. [16] to a Herschel-Bulkley fluid model. The dashed horizontal line is $\sigma(r_i)$ when $\sigma(6.7\text{ cm}) = \tau_o$ (black line) or $\sigma(6.3\text{ cm}) = \tau_o$ (gray line). The dotted line is $\sigma(r_i)$ when $\sigma(R) = \tau_o$. The vertical lines indicate the stress drops presented in Fig. 3 for $\Omega = 8 \times 10^{-4}$ rad/s.

Figure 2 shows $v(r)$ versus r for $\Omega = 5 \times 10^{-3}$ rad/s for a number of different averages. The solid circles represent an average over the entire flow regime (approximately 1000 s, starting 210 s after the initiation of shear). This will be referred to as the long-time average. Defining an event as a consecutive period of stress increase and decrease, the other curves are averaged over a single event (□), four events (○), 10 events (△), and 20 events (▽), respectively. The 10 event average is in reasonable agreement with the long-time average, and the 20 event average is indistinguishable from the long-time average. The

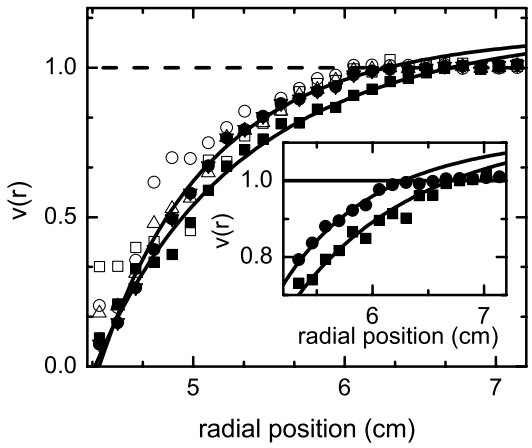

FIG. 2. $v(r) = v_\theta(r)/(r\Omega)$ versus r for $\Omega = 5 \times 10^{-3}$ rad/s averaged over time from $t = 250$ s to the end of the run (●) and for $\Omega = 8 \times 10^{-4}$ rad/s averaged over time from $t = 650$ s to the end of the run (■). The solid lines are fits to a power-law model for viscosity (see discussion in text). The dashed line is the $v = 1$ line. Also shown are $v(r)$ for $\Omega = 5 \times 10^{-3}$ rad/s averaged over a single event (□), four events (○), 10 events (△), and 20 events (▽). The inset shows the averages over the entire run in the region of the discontinuity for both shear rates (same symbols).

profiles for $\Omega = 8 \times 10^{-4}$ rad/s also converged rapidly, so Fig. 2 shows only the long-time average $v(r)$ for $\Omega = 8 \times 10^{-4}$ rad/s (approximately 1020 s, starting 650 s after the initiation of shear).

To find $\dot{\gamma}(r_c)$ and r_c, the average velocity is fit to $v(r) = A + B/r^{2/n}$ (solid curves) over the range $0 < v(r) < 0.98$, where $A = r_c^{2/n}/(r_c^{2/n} - r_i^{2/n})$ and $B = (r_i r_c)^{2/n}/(r_c^{2/n} - r_i^{2/n})$. This is the analytic solution for $v(r)$ for a power-law fluid [$\sigma(\dot{\gamma}) \propto \dot{\gamma}^n$] in a Couette geometry, with the outer radius taken as the critical radius r_c [1]. This form guarantees $v(r_c) = 1$ and $v(r_i) = 0$. Fitting A, B, and n determines r_i, r_c, and n. Because of the soft nature of the bubbles along the inner wall, r_i is left as a fitting parameter. However, for both fits, $r_i = 4.37 \pm 0.02$ cm. Unlike the expected solution for a Herschel-Bulkley fluid, there is a discontinuity in $\dot{\gamma}$ at r_c. In Fig. 2, the fit is extended past r_c to illustrate the discontinuity, which is highlighted by the inset in Fig. 2. Exponential fits to the data also do not accurately capture the discontinuity in shear rate at r_c because they correspond to a continuous shear rate. For $\Omega = 8 \times 10^{-4}$ rad/s, $r_c = 6.7$ cm, and $\dot{\gamma}(r_c) = 6 \times 10^{-4}$ s^{-1}. For $\Omega = 5 \times 10^{-3}$ rad/s, $r_c = 6.3$ cm, and $\dot{\gamma}(r_c) = 4 \times 10^{-3}$ s^{-1}. The difference in $\dot{\gamma}(r_c)$ for the two rotation speeds implies that, unlike discontinuous transition reported in Ref. [21], r_c is not set by a critical shear rate. The fits give $n = 0.45 \pm 0.05$ for $\Omega = 8 \times 10^{-4}$ rad/s and $n = 0.33 \pm 0.02$ for $\Omega = 5 \times 10^{-3}$ rad/s. For the faster rotation rate, the exponent is in agreement with the exponent in the Herschel-Bulkley fit to the stress [16] and velocity profiles measured at higher shear rates [22]. However, the measured exponent is different for the two rotation rates, as seen in other systems [6].

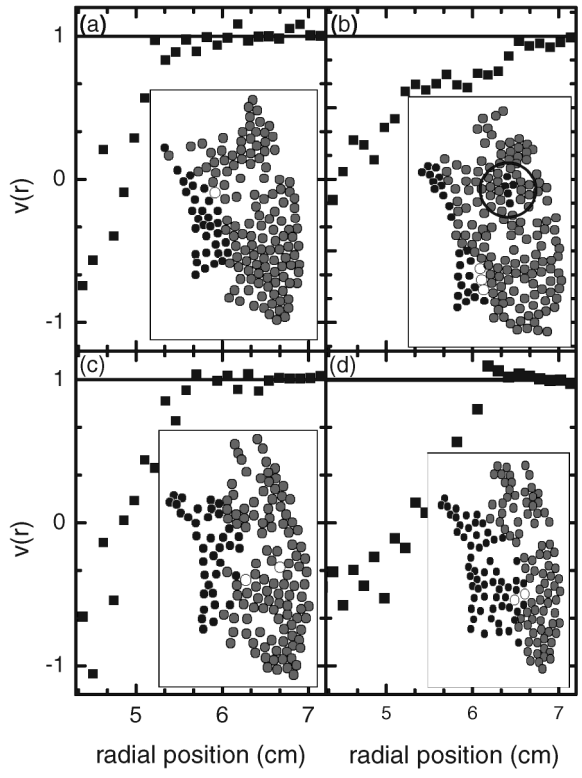

FIG. 3. Average velocity during the stress drops indicated in Fig. 1 for $\Omega = 8 \times 10^{-4}$ rad/s. The insets are images of a subset of the bubbles, with gray circles corresponding to $v(r)$ in the same direction as Ω, black circles corresponding to $v(r)$ opposite Ω, and white circles corresponding to $|v(r)| \leq 6 \times 10^{-4}$ cm/s.

Figure 3 presents plots of velocity profiles averaged over a single stress drop and corresponding snapshots of the bubble motions. The stress drops corresponding to Figs. 3(a)–3(d) are indicated by vertical lines in Fig. 1, labeled with corresponding letters. The individual velocity profiles are highly nonlinear and not consistent with a simple continuum model for viscosity. As expected, r_c fluctuates. However, the value of r_c is not consistent with two standard continuum assumptions: (1) $\sigma(r) = T/(2\pi r^2)$ (as expected for Couette flow [1]) and (2) $\langle \sigma(r_c) \rangle = \tau_o$, with τ_o determined from the fit to the Herschel-Bulkley model [16]. Under these continuum assumptions, stress drop (C) would have the largest value of r_c given its value of $\sigma(r_i)$. However, r_c is greater for both (D) and (B). This behavior is indicative of stress chains, or other nonuniform stress distributions, existing in the foam, similar to those observed for granular disks in two dimensions [9].

Figures 1 and 2 illustrate the connection between $\langle \sigma(r_i) \rangle$ and r_c determined from the time average velocity. The horizontal lines provide the expected values of $\langle \sigma(r_i) \rangle$ under the two previously listed continuum assumptions, for the relevant values of r_c. The solid dashed line is for $r_c = 6.7$ cm, which gives $\langle \sigma(r_i) \rangle = 2.06$ mN/m. The gray dashed line is for $r_c = 6.3$ cm, which gives $\langle \sigma(r_i) \rangle = 1.75$ mN/m. For comparison, the dotted line is $\sigma(r_i)$ such that $\sigma(R) = \tau_o$. For both runs, $\langle \sigma(r_i) \rangle = 1.82 \pm 0.01$ mN/m. The differences between the average stresses expected from the continuum assumptions and the actual average stresses are small, but significant. Additionally, the curves in Fig. 1 suggest that the maximum value of stress, which is higher for the run with larger r_c ($\Omega = 8 \times 10^{-4}$ rad/s), is potentially relevant. Further work into the connections between $\langle \sigma \rangle$ and r_c is needed.

Snapshots of the selected bubble motions are presented as insets in Fig. 3. The images are color coded so that bubbles moving opposite the outer cylinder (negative velocities) are black, gray bubbles are moving in the direction of rotation, and white bubbles have $|v(r)| \leq 6 \times 10^{-4}$ cm/s. The row of bubbles at each boundary is not shown. Bubble rearrangements are often discussed in terms of T1 events, or neighbor switching events. Detailed measurements of T1 events were beyond the scope of this work. However, bubbles with a negative velocity are indicative of such events. The snapshots in Fig. 3 reveal the qualitative connection between r_c and bubble rearrangements. For example, event (B) [Fig. 3(b)] possesses an isolated event at a relatively large radius (the

circled region). The signature of this in the velocity profile is the relatively large value of r_c and a plateau in the velocity profile where no bubbles with negative velocity are observed. In comparison, event (D) has a broad distribution of bubbles with negative velocities and a correspondingly smooth velocity profile.

Comparisons of the long-time velocity profiles (Fig. 2) and the velocities during a single stress drop (Fig. 3) reveal some interesting features. First, the bubble motion during stress drops, typically identified as periods of flow, exhibit a discontinuity in the shear rate and highly nonlinear velocity profiles. Averaging over a surprisingly small number of such events (10–20) produces a velocity profile that still has a discontinuity in shear rate at a critical radius r_c, but in the flowing region, the velocity profile is well described by a power-law fluid (a continuum model). Time averaging over even longer runs (50+ events) produces the same velocity profile (see Fig. 2), providing strong evidence that both the shear-rate discontinuity and the measured values of r_c are robust features of this system. Unlike the work in the continuum limit [6], r_c does not appear to be set by a critical shear rate (see discussion of Fig. 2). Measurements also rule out a simple connection between $\sigma(r_i)$ and r_c; therefore, if r_c is set by a critical stress, there must exist an inhomogeneous stress field (see discussion of Fig. 3). Other possibilities for the determining factor for r_c include the total strain experienced by bubbles and spatial correlations between nonlinear rearrangements. The question of what sets r_c will be the subject of future work.

The shear-rate discontinuity and corresponding velocity profiles observed in the low shear-rate limit discussed here are similar to those observed in other soft-matter systems at higher shear rates [6]. However, there is not enough information to determine why some systems exhibit discontinuous jamming transitions while shear localization in foam confined between glass plates [12] and granular systems [9–11,23] appears to be continuous. One intriguing possibility is the role of viscous dissipation. The dissipation mechanism in granular materials clearly differs from the bubble rafts reported on here. Also, the role of viscous dissipation in confined foam is probably very different from that in the bubble rafts. Recent simulations provide further support for the importance of viscous dissipation. These simulations did not include viscous dissipation in their models [24,25], but they do report shear localization in which the shear rate is continuous. Further studies of this question will be important for deepening our understanding of the general applicability of the jamming phase diagram concept.

This work was supported by Department of Energy Grant No. DE-FG02-03ED46071, the Research Corporation, and Alfred P. Sloan Foundation. J. L. thanks UROP and NSF Grant No. PHY-9988066 for additional funding. The authors thank Corey O'Hern and Phillipe Coussot for useful discussions.

*Present address: Naval Surface Warfare Center Corona Division QA-32, Corona, CA 92878-5000, USA.
†Present address: Stanford University, P.O. Box 11878, Stanford, CA 94309, USA.

[1] Various books cover both the modeling and experimental measurement of yield stress materials and complex fluids in general. Two examples are R. B. Bird, R. C. Armstrong, and O. Hassage, *Dynamics of Polymer Liquids* (Wiley, New York, 1977) and C. Macosko, *Rheology Principles, Measurements, and Applications* (VCH Publishers, New York, 1994).
[2] *Jamming and Rheology: Constrained Dynamics on Microscopic and Macroscopic Scales*, edited by A. J. Liu and S. R. Nagel (Taylor & Francis, New York, 2001).
[3] A. J. Liu and S. R. Nagel, Nature (London) **396**, 21 (1998).
[4] V. Trappe, V. Prasad, L. Cipelletti, P. N. Segre, and D. A. Weitz, Nature (London) **411**, 772 (2001).
[5] P. Coussot, Q. D. Nguyen, H. T. Huynh, and D. Bonn, Phys. Rev. Lett. **88**, 175501 (2002).
[6] P. Coussot, J. S. Raynaud, F. Bertrand, P. Moucheront, J. P. Guilbaud, H. T. Huynh, S. Jarny, and D. Lesueur, Phys. Rev. Lett. **88**, 218301 (2002).
[7] F. DaCruz, F. Chevoir, D. Bonn, and P. Coussot, Phys. Rev. E **66**, 051305 (2002).
[8] J.-B. Salmon, A. Colin, S. Manneville, and F. Molino, Phys. Rev. Lett. **90**, 228303 (2003).
[9] D. Howell, R. P. Behringer, and C. Veje, Phys. Rev. Lett. **82**, 5241 (1999).
[10] D. M. Mueth, G. F. Debregeas, G. S. Karczmar, P. J. Eng, S. R. Nagel, and H. M. Jaeger, Nature (London) **406**, 385 (2000).
[11] W. Losert, L. Bocquet, T. C. Lubensky, and J. P. Gollub, Phys. Rev. Lett. **85**, 1428 (2000).
[12] G. Debrégeas, H. Tabuteau, and J. M. di Meglio, Phys. Rev. Lett. **87**, 178305 (2001).
[13] J.-B. Salmon, L. Bécu, S. Manneville, and A. Colin, Eur. Phys. J. E **10**, 209 (2003).
[14] H. M. Princen, J. Colloid Interface Sci. **105**, 150 (1985).
[15] T. G. Mason, J. Bibette, and D. A. Weitz, J. Colloid Interface Sci. **179**, 439 (1996).
[16] E. Pratt and M. Dennin, Phys. Rev. E **67**, 051402 (2003).
[17] S. Tewari, D. Schiemann, D. J. Durian, C. M. Knobler, S. A. Langer, and A. J. Liu, Phys. Rev. E **60**, 4385 (1999).
[18] D. Lootens, H. VanDamme, and P. Hébraud, Phys. Rev. Lett. **90**, 178301 (2003).
[19] A. S. Argon and H. Y. Kuo, Mater. Sci. Eng. **39**, 101 (1979).
[20] R. S. Ghaskadvi and M. Dennin, Rev. Sci. Instrum. **69**, 3568 (1998).
[21] S. Rodts, J. C. Baudez, and P. Coussot, report, 2003 (to be published).
[22] J. Lauridsen, M. Twardos, and M. Dennin, Phys. Rev. Lett. **89**, 098303 (2002).
[23] L. Bocquet, W. Losert, D. Schalk, T. C. Lubensky, and J. P. Gollub, Phys. Rev. E **65**, 011307 (2001).
[24] F. Varnik, L. Bocquet, J.-L. Barrat, and L. Berthier, Phys. Rev. Lett. **90**, 095702 (2003).
[25] A. Kabla and G. Debrégeas, Phys. Rev. Lett. **90**, 258303 (2003).